*J. Numer. Math.*, Vol. 0, No. 0, pp. 1–15 (2012)
DOI 10.1515/ JNUM.2012.000
 *Prepared using* jnm.sty *[Version: 20.02.2007 v1.3]*

# A finite element BFGS algorithm for the reconstruction of the flow field generated by vortex rings

Y. ZHANG,* I. DANAILA*

*Received* *Communicated by*
*Received in revised form*

**Abstract** — Vortex rings are generated in numerous practical applications (biological propulsion, internal combustion engines) by the sudden injection of a fluid. Measurements of such flows often provide partial information, generally limited to the exterior of the vortex ring. We propose in this paper a new algorithm for the reconstruction of the stream function inside a bounded domain, where a vortex ring is supposed to form. We derive a quasi-Newton Broyden-Fletcher-Goldfarb-Shanno (BFGS) algorithm for this problem, using a cost function that describes the matching between the reconstructed field and given values of normal derivatives on the boundary of the domain. The algorithm computes the best parameters of the vortex model that is used to describe the vorticity distribution inside the vortex ring. Several vortex models are considered. The method is implemented in FreeFem++ using a $P^1$ finite-element spatial discretization. Validation tests using analytical models (Hill's spherical vortex) and Navier-Stokes direct numerical simulation data show good agreement between reconstructed and reference fields.

**Keywords:** Vortex ring models, Finite element methods, Reconstruction, BFGS

## 1. Introduction

Vortex-ring flows are fundamentally significant [4,28,1] for many practical applications in fluid mechanics, ranging from biological propulsion problems [8,24,22] to the study of fuel injection in automobile engines [5,19,11]. For the latter application, PIV (Particle Image Velocimetry) measurements of the injected two-phase flow do not provide reliable velocity vectors in the core of the vortex ring, because of the high density of seeding particles. It is then necessary to theoretically reconstruct the flow field not accessible by measurements. The present contribution is, to the best of our knowledge, the first attempt to develop an effective algorithm for the reconstruction of the velocity field associated to vortex ring flows, using only the outside-core available information. A similar field reconstruction problem from partial measurements is encountered in the study of Tokamak plasma reactors [7].

*Laboratoire de Mathématiques Raphaël Salem, Université de Rouen, F-76801 Saint-Étienne-du-Rouvray, France

This work was supported by the Program MAGIE-FUI7 Pôle MOVEO.

Vortex rings were extensively studied in the mathematical [2,15,13,6] and physical literature [26,14,20,12] as fundamental solutions of Euler equations. The vortex ring problem is displayed in Fig. 1. The flow is supposed to be axisymmetric and thus described in cylindrical coordinates, with ($z$, $r$, $\vartheta$) denoting the longitudinal, radial and azimuthal direction of the flow, respectively. We also consider that the motion is steady in a reference frame translating with the vortex ring velocity $W$ (assumed constant). Let $\psi$ denote the Stokes stream function in this reference frame. The advantage of this description is that inside the vortex ring the fluid circulates over closed streamlines $\psi = const.$, while the streamlines are open for the external flow (see Fig. 1a). The vortex bubble $\Omega_b$ is defined by the dividing streamline ($\psi = 0$) ; the flow outside the bubble is generally considered as a potential flow. The vorticity is concentrated in the vortex core $\Omega_c$ and is zero elsewhere. It is generally assumed that the vortex core boundary $\partial\Omega_c$ is a streamline $\psi = k$, with $k$ a positive constant. Physically, $2\pi k$ represents the flow rate between the axis $Oz$ and $\partial\Omega_c$. On the axis of symmetry ($r = 0$) the radial velocity is $v_r = 0$ and consequently $\psi = 0$.

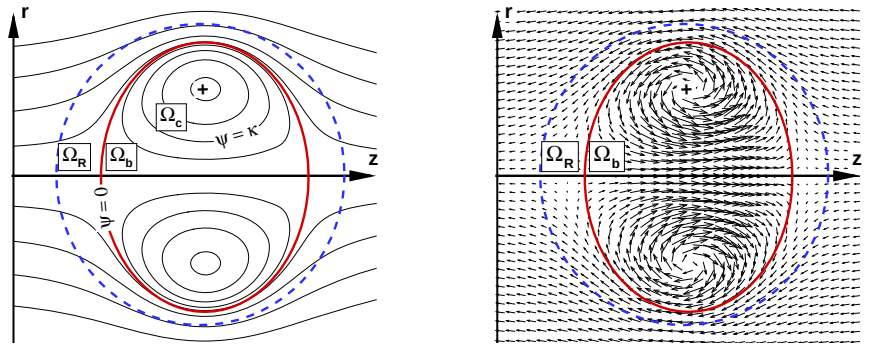


(a) (b)

**Figure 1.** Direct numerical simulation (DNS) of the physical vortex ring by solving the incompressible Navier-Stokes equations [9]. (a) Streamlines in the reference frame travelling with the vortex ring velocity $W$. (b) Velocity vectors in the same reference frame. Boundaries of the vortex bubble $\Omega_b$ (continuous thick red line) and the reconstruction domain $\Omega_R$ (dashed blue line).

For the reconstruction problem, the streamline $\psi$ (or velocity vectors) are not known inside the domain $\Omega_R$ displayed in Fig. 1. Supposing that measurements (or DNS) provide streamline values $\psi_{\text{exp}}$ on $\partial\Omega_R$ and outside $\Omega_R$, we develop in this paper an algorithm to reconstruct the missing flow field inside $\Omega_R$.

The mathematical difficulty of the reconstruction problem comes from the non-uniqueness of the vortex-ring solution that could be used to fill the missing field. Such models generally require fitting parameters based upon integral quantities (circulation, impulse and energy) and assume a particular vorticity distribution in the core. Our reconstruction procedure starts from a particular vortex ring model

with given circulation (assumed known from measurements or other estimations, *e. g.* slug-flow models) and compute the other parameters of the model by solving an associated optimal control problem. For this problem we first define a suitable cost function describing the match between the velocity field induced by the vortex and the prescribed external field. The cost function is then minimized using a quasi-Newton Broyden-Fletcher-Goldfarb-Shanno (BFGS) method based on finite-element spatial discretization. Different vortex models are analysed, based on classical Norbury-Fraenkel model [26], or Kaplanski-Rudi model [20,21].

The algorithm will be tested using DNS vortex-ring data [9,10] obtained by solving the Navier-Stokes equations in cylindrical coordinates. The velocity field $(v_z, v_r)$ obtained from DNS (an example is shown in Fig. 1) will be used to compute the reference stream function $\psi_{\text{exp}}$ by solving the equation $\mathscr{L}\psi_{\text{exp}} = \partial v_z/\partial r - \partial v_r/\partial z$ with Dirichlet boundary conditions and $\mathscr{L}$ defined below.

## 2. Mathematical problem

The problem of the inviscid, steady vortex ring is defined by:

$$\mathscr{L}\psi = \begin{cases} \omega_0 f\left(r, \psi + \dfrac{1}{2}Wr^2\right), & \text{in} \quad \Omega_c \\ 0, & \text{in} \quad \Pi\backslash\bar{\Omega}_c, \end{cases} \tag{2.1}$$

where $\Pi = \{(z,r)|r>0\}$ is the half-plane and $\mathscr{L}$ is a self-adjoint elliptic operator given by:

$$\mathscr{L} = -\left(\frac{\partial}{\partial z}\left(\frac{1}{r}\frac{\partial}{\partial z}\right) + \frac{\partial}{\partial r}\left(\frac{1}{r}\frac{\partial}{\partial r}\right)\right) = -\nabla\cdot\left(\frac{1}{r}\nabla\right), \tag{2.2}$$

with $\nabla = \left(\dfrac{\partial}{\partial z}, \dfrac{\partial}{\partial r}\right)^t$. We note that $\mathscr{L}(\frac{1}{2}Wr^2 + k) = 0$, with $W$ and $k$ real constants.

The additional constraints on the solution are (see Fig. 1):

$$\psi \text{ and } \nabla\psi \text{ are continuous across } \partial\Omega_c, \tag{2.3}$$

$$\psi = k \quad \text{on} \quad \partial\Omega_c, \quad \psi = 0 \quad \text{on} \quad Oz, \tag{2.4}$$

$$\psi + \frac{1}{2}Wr^2 \to 0 \quad \text{when} \quad r^2 + z^2 \to \infty. \tag{2.5}$$

There are four parameters of the problem: $W$, the translation velocity (assumed constant), $k$, the flux constant, $\omega_0$, the vortex strength (constant) and $f(r,\psi)$, the vorticity function. An additional constraint could be imposed [15] by prescribing the kinetic energy of the vortex ring:

$$\eta = \int_\Pi (v_r^2 + v_z^2)\, r\mathrm{d}r\mathrm{d}z = \int_\Pi \frac{1}{r}|\nabla\psi|^2\, \mathrm{d}r\mathrm{d}z. \tag{2.6}$$

Generally, the constant $\omega_0$ and the vorticity function $f(r,\psi)$ are prescribed by, what is called, a vortex ring model (see below). As a consequence, two different formulations of the vortex ring problem are possible (see also [6]):
*(i) the free vortex velocity problem*: given $\eta > 0$ and $k \geqslant 0$, find $\psi$ and $W > 0$, satisfying (2.1),
*(i) the free flux parameter problem*: given $\eta > 0$ and $W > 0$, find $\psi$ and $k \geqslant 0$, satisfying (2.1).
For a discussion of mathematical results on the existence and uniqueness of solutions of these two problems, we refer to [3,15,6].

It is interesting to note that the main difficulty in solving these problems comes from the fact that the boundary $\partial\Omega_c$ is not known, which makes it a *free boundary problem*. The problem could be reduced to a semi-linear elliptic problem [15] by extending $f$ as

$$f(r,\psi) > 0, \quad \forall \psi \geqslant k, \qquad \text{and} \qquad f(r,\psi) = 0, \quad \forall \psi < k. \tag{2.7}$$

It results, by the maximum principle, that the vortex core $\Omega_c$ could be defined as:

$$\Omega_c = \{\mathbf{x} \in \Pi; \psi(\mathbf{x}) \geqslant k\}, \tag{2.8}$$

and (2.1) is equivalent to

$$\mathscr{L}\psi = \omega_0 f\left(r, \psi + \frac{1}{2}Wr^2\right)\chi_{\psi(\mathbf{x})\geqslant k}, \quad \text{in} \quad \Pi, \tag{2.9}$$

where $\chi_{\psi(\mathbf{x})\geqslant k}$ is the characteristic function of the domain $\Omega_c$.

## 3. The optimal control problem

Before introducing the optimal control problem, we define the function space [15]

$$H_0(\Omega) = \left\{ u \in L^2(\Omega) : \frac{1}{r}|\nabla u|^2 \in L^1(\Omega) \mid u = 0 \text{ on } \Gamma = \partial\Omega \right\}. \tag{3.1}$$

$H_0(\Omega)$ is the closure of the standard test function space for the Hilbert norm

$$\|u\|_{H_0(\Omega)} = \left( \int_\Omega |u|^2 \mathrm{d}\tau + \int_\Omega \frac{1}{r^2}|\nabla u|^2 \,\mathrm{d}\tau \right)^{1/2}, \quad \mathrm{d}\tau = r\mathrm{d}r\mathrm{d}z \tag{3.2}$$

It is interesting to note that the semi-norm

$$\|u\| = \left( \int_\Omega \frac{1}{r^2}|\nabla u|^2 \,\mathrm{d}\tau \right)^{1/2} = \left( \int_\Omega \frac{1}{r}|\nabla u|^2 \,\mathrm{dx} \right)^{1/2}, \quad \mathrm{dx} = \mathrm{d}r\mathrm{d}z, \ \mathrm{x} = (r,z), \tag{3.3}$$

is in fact a norm on $H_0(\Omega)$, equivalent to the norm (3.2) [6,15], and hence

$$a(u,v) = \int_\Omega \frac{1}{r}\nabla u \cdot \nabla v \,\mathrm{dx}, \tag{3.4}$$

is an elliptic symmetric bilinear form corresponding to the inner product $< u,v >= a(u,v)$ in $H_0(\Omega)$. We consider in the following the space $H_0(\Omega)$ equipped with the inner product inducing the norm (3.3); this is a natural setting for the problem (2.1), since

$$< u,v >= \int_\Omega \frac{1}{r}\nabla u \cdot \nabla v \,\mathrm{d}\mathrm{x} = \int_\Omega v\mathscr{L}u \,\mathrm{d}\mathrm{x}, \quad \text{for} \quad u \in H_0(\Omega), v \in H_0(\Omega)\cap C^2(\overline{\Omega}). \tag{3.5}$$

Considering $\Omega \subset \Pi$ a bounded domain with a smooth boundary $\partial\Omega$, we introduce now the following general vortex ring problem:

$$\begin{cases} \mathscr{L}\psi = \omega_0 f(\mathrm{x},\psi,\mathrm{X}), \text{ in } \quad \Omega, \\ \psi(\mathrm{x}) = g(\mathrm{x}), \qquad\qquad \text{on } \partial\Omega, \end{cases} \tag{3.6}$$

where $f(\mathrm{x},\psi,\mathrm{X})$ is the generalized vorticity function and X the set of parameters describing the vorticity function. In several vortex models, the function $f$ is discontinuous, with $f(\mathrm{x},\cdot,\cdot) \neq 0,\ \mathrm{x} \in \Omega_c$ and $f(\mathrm{x},\cdot,\cdot) = 0,\ \mathrm{x} \in \Omega \setminus \Omega_c$. As a consequence, the stream function is $\psi \in C^1(\overline{\Omega})\cap C^2(\overline{\Omega}\setminus\partial\Omega_c)$. The requirement that $\psi$ is $C^1$ across the boundary of the vortex core ensures the continuity of the velocity $\mathbf{v}$.

Assuming that $g(\mathrm{x}) = 0$ and using the scalar product (3.5), the corresponding variational form is given by

$$\begin{cases} \text{Find: } \psi \in H_0(\Omega) \text{ such that} \\ < \psi,\varphi >= (\omega_0 f(\mathrm{x},\psi,\mathrm{X}),\varphi),\ \forall\varphi \in H_0(\Omega), \end{cases} \tag{3.7}$$

where $(\cdot,\cdot)$ denotes the $L^2(\Omega)$ scalar product. If $g(\mathrm{x}) \neq 0$, we can set $\psi(\mathrm{x}) := \psi(\mathrm{x}) - g(\mathrm{x})$ and get the similar variational problem (3.7) with the homogeneous boundary condition.

For the reconstruction model, $\Omega = \Omega_R$, and the vorticity function $f$ is prescribed by a vortex ring model based on physical or mathematical considerations. The values of parameters $X$ must guarantee the existence of a vortex ring that best matches the external given field. It is important to note that the vortex strength $\omega_0$ is an adjustable parameter that is generally prescribed by imposing physical characteristics of the vortex ring. Indeed, since the vorticity of the vortex ring is $\omega = \omega_0 f(\mathrm{x},\psi,\mathrm{X})$, the main integral quantities describing the flow are the circulation $\Gamma$, the hydrodynamic impulse $I$ and the energy $E$:

$$\Gamma = \int \omega \mathrm{d}r\mathrm{d}z,\ I = \pi\int \omega r^2 \mathrm{d}r\mathrm{d}z,\ E = \pi\int \omega\psi \mathrm{d}r\mathrm{d}z. \tag{3.8}$$

We choose in the following to prescribe the circulation of the vortex ring (from experiments or DNS simulations), which is generally the approach used in physical modeling of such flows. Formally, $\omega_0$ is determined from

$$\Gamma_{\text{exp}} = \int_{\partial\Omega} \frac{1}{r}\frac{\partial\psi_{\text{exp}}}{\partial\mathbf{n}}\mathrm{d}S = \omega_0 \int_\Omega f(\mathrm{x},\psi,\mathrm{X})\mathrm{d}r\mathrm{d}z. \tag{3.9}$$

The set of $p$ parameters $X \in \mathbb{R}^p$ will be determined from the following optimal control problem:

$$\underset{\mathrm{X}\in\mathbb{R}^n}{\mathrm{Min}}\ J(\psi) = \int_{\partial\Omega_R} \left| \frac{1}{r}\left( \frac{\partial \psi}{\partial \mathbf{n}} - \frac{\partial \psi_{\text{exp}}}{\partial \mathbf{n}} \right) \right|^2 \mathrm{d}S \tag{3.10}$$

subject to

$$\begin{cases} \mathscr{L}\psi = \omega_0 f(\mathrm{x}, \psi, \mathrm{X}), & \text{in } \Omega_\mathrm{R}, \\ \psi = \psi_{\text{exp}}, & \text{on } \partial\Omega_R. \end{cases} \tag{3.11}$$

The quantity $\frac{1}{r}\frac{\partial \psi}{\partial \mathbf{n}} = \frac{1}{r}\nabla\psi\cdot\mathbf{n} = \mathbf{v}\cdot\tau$ represents the tangential velocity to the boundary $\partial\Omega_R$. When the boundary of the domain is a streamline, the normal component of the velocity is zero, and thus, our formulation enforces the constraint of the continuity of the velocity across $\partial\Omega_R$.

In order to solve the optimization problem, the gradient of the cost function $J(\cdot)$ will be needed. We use the adjoint method (*e. g.* [29,27]) to compute the variational derivatives of $J(\cdot)$ with respect to $X_i, i = 1,\ldots,p$:

$$\frac{\delta J}{\delta X_i} = \frac{\delta J}{\delta \psi}\frac{\delta \psi}{\delta X_i} = 2\int_{\partial\Omega} \frac{1}{r^2}\left( \frac{\partial \psi}{\partial \mathbf{n}} - \frac{\partial \psi_{\text{exp}}}{\partial \mathbf{n}} \right) \frac{\partial}{\partial \mathbf{n}}\left( \frac{\delta \psi}{\delta X_i} \right) \mathrm{d}S \tag{3.12}$$

The quantities $\delta\psi/\delta X_i$ can be calculated from (3.11) as follows

$$\begin{cases} \mathscr{L}\left( \dfrac{\delta \psi}{\delta X_i} \right) = \omega_0 \dfrac{\delta f(\mathrm{x}, \psi, \mathrm{X})}{\delta X_i}, & \text{in } \Omega, \\ \dfrac{\delta \psi}{\delta X_i} = 0, & \text{on } \partial\Omega. \end{cases} \tag{3.13}$$

### 3.1. The quasi-Newton BFGS algorithm

The minimization problem (3.10) is solved using the modified quasi-Newton Broyden-Fletcher-Goldfarb-Shanno (BFGS) algorithm (*e. g.* [18]):

1. Set an initial guess $X^{(0)}$ of the $p$ parameters and $\psi^{(0)}$. Initialize the iteration tolerances $\text{eps}_J$, $\text{eps}_X$ and the maximum iteration steps $N$.
2. Use the experimental data $\psi_{\text{exp}}$ on $\partial\Omega_R$ to calculate $\Gamma_{\text{exp}}$ from (3.9) and get $\omega_0^{(n)}$ from the same equation.
3. Solve (3.11) and obtain $\psi^{(n)}$. Note that in the case of a vorticity function $f$ depending on the solution $\psi$ itself, equation (3.11) is non-linear and specific algorithms must be used (see next section). Particular attention must be paid when $f$ is discontinuous; a numerical algorithm for such cases is proposed in [11].

4. Get $\nabla J(\psi^{(n)})$ by the following equation

$$\nabla_{\psi} J \cdot \delta\psi^{(n)} = 2 \cdot \int_{\partial\Omega_R} \frac{1}{r^2} \left( \frac{\partial \psi^{(n)}}{\partial \mathbf{n}} - \frac{\partial \psi_{\exp}}{\partial \mathbf{n}} \right) \cdot \frac{\partial(\delta\psi^{(n)})}{\partial \mathbf{n}} \mathrm{d}z\mathrm{d}r. \tag{3.14}$$

From (3.11), we can compute

$$\mathscr{L}\left( \frac{\partial \psi^{(n)}}{\partial X_i} \right) = \omega_0^{(n)} \left. \frac{\partial f(\psi^{(n)}, X)}{\partial X_i} \right|_{X=X^{(n)}}. \tag{3.15}$$

with homogeneous Dirichlet boudary conditions:

$$\frac{\partial \psi^{(n)}}{\partial X_i} = 0, \text{ on } \partial\Omega_R. \tag{3.16}$$

Then, $\nabla_X J(\psi^{(n)})$ is calculated from (3.14)

$$\nabla_X J(\psi^{(n)}) = \left\{ \nabla_{\psi} J \cdot \left( \frac{\partial \psi^{(n)}}{\partial X_i} \right) \right\}_{i=0,\ldots,p}. \tag{3.17}$$

5. Compute the maximum acceptable Euclidean norm of the gradient $\|\nabla_X J(\psi^n)\|$. If $\|\nabla_X J(\psi^n)\| \leqslant \mathrm{eps}_J$, the iteration is terminated. Otherwise, the following Step 6 is implemented.

6. Using the Hessian matrix $H\left(\psi^{(n+1)}\right)$, we have

$$\nabla_X J\left(\psi^{(n+1)}\right) \approx \nabla_X J\left(\psi^{(n)}\right) + H\left(\psi^{(n+1)}\right) \cdot \delta X^{(n+1)}. \tag{3.18}$$

If (3.18) is equal to zero, we obtain

$$\delta X^{*,(n)} = -H^{-1}\left(\psi^{(n+1)}\right) \cdot \nabla_X J\left(\psi^{(n)}\right). \tag{3.19}$$

We can thus update $X^{(n+1)}$ by

$$X^{(n+1)} = X^{(n)} + \beta^{(n)} X^{*,(n)}, \tag{3.20}$$

where $\beta^{(n)}$ is an acceptable step size in the direction $\delta X^{*,(n)}$ obtained by a line search algorithm.

7. $H\left(\psi^{(n+1)}\right)$ is obtained by the classical BFGS method [18] as follows

$$H\left(\psi^{(n+1)}\right) = H\left(\psi^{(n)}\right) + \frac{Y^{(n)} Y^{(n),T}}{Y^{(n),T} \delta X^{(n)}} - \frac{H\left(\psi^{(n)}\right) \delta X^{(n)} (H\left(\psi^{(n)}\right) \delta X^{(n)})^T}{\delta X^{(n),T} H\left(\psi^{(n)}\right) \delta X^{(n)}}, \tag{3.21}$$

and $H^{-1}\left(\psi^{(n+1)}\right)$ is calculated by

$$H^{-1}\left(\psi^{(n+1)}\right) = \left(I - \frac{Y^{(n)}\delta X^{(n),T}}{Y^{(n),T}\delta X^{(n)}}\right)^T H^{-1}\left(\psi^{(n)}\right)\left(I - \frac{Y^{(n)}\delta X^{(n),T}}{Y^{(n),T}\delta X^{(n)}}\right) + \frac{\delta X^{(n)}\delta X^{(n),T}}{Y^{(n),T}\delta X^{(n)}} \tag{3.22}$$

where $Y^{(n)}$ and $\delta X^{(n)}$ are defined by

$$Y^{(n)} = \nabla_X J\left(\psi^{(n+1)}\right) - \nabla_X J\left(\psi^{(n)}\right),\ \delta X^{(n)} = \beta^{(n)}\delta X^{*,(n)}. \tag{3.23}$$

8. If $\left\|X^{(n+1)} - X^{(n)}\right\| / \left\|X^{(n)}\right\| \leqslant \mathrm{eps_X}$ or $n+1 > N$, the iteration is terminated. Otherwise, go to Step 2.

### 3.2. Vortex models and comparison with DNS data

In this section we review the vortex ring models giving the form of the vorticity function $f$ and compute the derivatives needed in the previous section. We refer to Fig. 1 for the geometrical definition of the problem. The ability of the models to describe real vortex ring flows was evaluated using direct numerical simulation (DNS) in [9].

#### 3.2.1. The Kaplanski-Rudi viscous vortex model and Gaussian-type models.

Extensive comparisons between analytical vortex ring models and DNS data [9] showed that the model proposed by Kaplanski and Rudi [20] is the most realistic since it takes into account the viscosity of the flow. As a consequence, in the classical Kaplanskin-Rudi model, the vorticity distribution is continuous and assumed to possess the following Gaussian shape:

$$\omega = \omega_0 f, \quad f = \exp\left[-\frac{1}{2}\left(\sigma^2+\eta^2+\tau^2\right)\right]\mathbf{I}_1(\sigma\tau), \tag{3.24}$$

where $l$ is a viscous length scale, $\sigma = r/l$, $\eta = [z - Z_c(t)]/l$ and $Z_c$ the axial coordinate of the vortex center. $\mathbf{I}_1$ is the first-order modified Bessel function. The original fitting method is presented in [9] using physical considerations.

The main drawback of this model is that the Gaussian distribution (3.24) is isotropic and does not take into account the real non-isotropic distribution of the vorticity in the vortex core. A modification of the model based on this consideration will consider the following vorticity distribution:

$$\omega = \omega_0 f, \quad f = \exp\left[-\alpha_R^2(r-Rc)^2 - \alpha_Z^2(z-Zc)^2\right]. \tag{3.25}$$

If $\alpha_R = \alpha_Z = \alpha$, we have

$$\omega = \omega_0 f, \quad f = \exp\left[-\alpha^2((r-Rc)^2 + (z-Zc)^2)\right]. \tag{3.26}$$

**3.2.2. The smoothed Norbury-Fraenkel-type model.** One of the most popular vortex ring models used in Fluid Mechanics is the Norbury-Fraenkel model [14,26] assuming that $f$ is a discontinuous function $f = rH(\mathbf{x})$, with $H$ the Heaviside function $H|_{\Omega_c} = 1, H|_{\Pi\setminus\Omega_c} = 0$. The limiting case for $k = 0$ (see Fig. 1) corresponds to a vortex core occupying the entire vortex bubble, *i. e.* $\Omega_c = \Omega_b$; when $\Omega_c$ is a sphere, we obtain the Hill's spherical vortex [17,23,4]. It is easy to notice that in this case, the equation (2.9) becomes a nonlinear eigenvalue problem. Existence and uniqueness results for this problem are presented in [15,3] for the general case and in [2,25] for vortex rings bifurcating from Hill's vortex. Norbury [26] numerically computed a family of such vortex rings by introducing a single geometric parameter; this model is nowadays largely used to describe real vortex rings generated experimentally [8] or numerically [9,10].

Since we intend to set a unified numerical approach for different vortex models, we have supposed in the previous section that the vorticity function $f$ is continuous and derivable. Consequently, we propose a regularization of the original vorticity function by the following smoothed function (see also [6]):

$$f_\varepsilon(\psi,k) = \frac{r}{2}\left(1 + \frac{\psi - k}{\sqrt{(\psi-k)^2+\varepsilon}}\right), \tag{3.27}$$

where $\varepsilon \in \mathbb{R}^+$. It is easy to validate the following approximation relation

$$\lim_{\varepsilon\to 0^+} f_\varepsilon(\psi,k) = f(\psi,k). \tag{3.28}$$

In order to guarantee $k \geqslant 0$, let $k = \alpha^2$ in (3.27). Then, the following formulation is proposed for approaching the problem (3.11)

$$\begin{cases} \mathscr{L}\psi_\varepsilon = \omega_0 f_\varepsilon(\psi,\alpha), & \text{in } \Omega_R, \\ \psi_\varepsilon = \psi_{\exp}, & \text{on } \partial\Omega_R. \end{cases} \tag{3.29}$$

In order to solve (3.29) effectively for the Step 3 of our algorithm, the Newton iteration method is employed. The linearized iteration form is given as follows

$$\mathscr{L}\psi_\varepsilon^{(n)} = \omega_0 f_\varepsilon\left(\psi^{(n-1)},\alpha\right) + \omega_0 \left.\frac{\partial f_\varepsilon(\psi,\alpha)}{\partial\psi}\right|_{\psi=\psi^{(n-1)}} (\psi^{(n)} - \psi^{(n-1)}). \tag{3.30}$$

Corresponding to (3.15), we have the following form

$$\begin{aligned} \mathscr{L}\left(\frac{\partial\psi_\varepsilon^{(n)}}{\partial\alpha}\right) = {} & \omega_0 \left.\frac{\partial f_\varepsilon(\psi_\varepsilon,\alpha)}{\partial\psi_\varepsilon}\right|_{\psi_\varepsilon=\psi_\varepsilon^{(n)},\omega_0=\omega_0^{(n)},\alpha=\alpha^{(n-1)}} \frac{\partial\psi_\varepsilon^{(n)}}{\partial\alpha} + \\ & \omega_0 \left.\frac{\partial f_\varepsilon(\psi_\varepsilon,\alpha)}{\partial\alpha}\right|_{\psi_\varepsilon=\psi_\varepsilon^{(n)},\omega_0=\omega_0^{(n)},\alpha=\alpha^{(n-1)}}. \end{aligned} \tag{3.31}$$

Using (3.30) and (3.31), the BFGS algorithm given in Sec. 3.1 can be applied for the reconstruction problem based on the regularized Norbury-Fraenkel vortex ring model.

### 3.3. Numerical validations

We show here numerical results on the flow field reconstruction using the BFGS algorithm described in section 3.1. The algorithm is implemented in FreeFem++ using $P^1$ finite elements. It is important to observe that the bilinear form (3.4) appearing in (3.11) and (3.13) is singular at $r = 0$. This imposes a modification of the finite-element basis functions when a triangle possesses a vertex on the axis $Oz$, as proposed in [6]. An equivalent treatment is applied here, since the quadrature formulas used in FreeFem++ are by default of fifth order and, consequently, the integrands values are automatically set to zero for vertices on the $Oz$ axis. With this modification, the standard finite element analysis could be applied to our problem (see [6] for details).

**3.3.1. Validation using analytical solutions: reconstruction of Hill's spherical vortex by the smoothed Norbury-Fraenkel model.** The Hill's spherical vortex is a validation case, since we know the analytical solution. This vortex is a limit case in which $\Omega_c = \Omega_b$ is a sphere (see Fig. 1) and the vorticity distribution is

$$\omega = \begin{cases} Cr, \text{ if } r^2+z^2 \leqslant a^2, \\ 0, \quad \text{if } r^2+z^2 > a^2. \end{cases} \tag{3.32}$$

By matching the solution inside the sphere with the external solution describing an uniform flow of velocity $W$, the following compatibility relationship is obtained: $W = \dfrac{2}{15}Ca^2$. The complete solution [4,28,23] in the frame of reference traveling with the translation velocity $W$ is:

$$\psi(r,z) = \begin{cases} \dfrac{C}{10}r^2(a^2-r^2-z^2), & \text{if } r^2+z^2 \leqslant a^2, \\ \dfrac{Cr^2a^2}{15}\left(\dfrac{a^3}{(r^2+z^2)^{3/2}}-1\right), & \text{if } r^2+z^2 > a^2. \end{cases} \tag{3.33}$$

$$v_r(r,z) = \begin{cases} \dfrac{C}{5}rz, & \text{if } r^2+z^2 \leqslant a^2, \\ \dfrac{Ca^5}{5}\dfrac{rz}{(r^2+z^2)^{5/2}}, & \text{if } r^2+z^2 > a^2, \end{cases} \tag{3.34}$$

$$v_z(r,z) = \begin{cases} -\dfrac{C}{5}(2r^2+z^2-a^2), & \text{if } r^2+z^2 \leqslant a^2, \\ -\dfrac{Ca^5}{15}\left[\dfrac{r^2-2z^2}{(r^2+z^2)^{5/2}}+\frac{2}{a^3}\right], & \text{if } r^2+z^2 > a^2, \end{cases} \tag{3.35}$$

It is possible to calculate the invariants of motion for the Hill's vortex, and the following non-dimensional quantities are useful to validate the numerical system:

$$\frac{\Gamma}{Wa} = 5, \quad \frac{I}{Wa^3} = 2\pi, \quad \frac{E}{W^2a^3} = \frac{3}{7}\pi. \tag{3.36}$$

We first compute the vortex ring solution using our finite element solver. The solution is displayed in Fig. 2 for a large domain including the spherical vortex and the exterior (rectangular) domain.

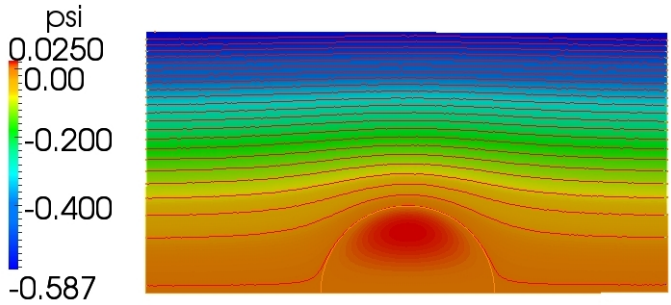


**Figure 2.** Computed stream function for Hill's vortex.

**Table 1.** Relative errors for the integrals of motion: circulation, impulse and energy given by (3.36). The mesh of the exterior domain is constant and has $N_t^{\text{ext}} = 36407$ triangles and $h^{\text{ext}} = 0.123936$.

| $N_t^{\text{int}}$ | $h^{\text{int}}$ | $W$ | $\Gamma/(Wa)$ | $I/(Wa^3)$ | $E/(W^2a^3)$ |
|---|---|---|---|---|---|
| 8599 | 0.033452 | 1.117e-3 | 1.02298e-3 | 9.56182e-4 | 2.01207e-3 |
| 34514 | 0.020746 | 1.275e-4 | 1.01334e-4 | 8.46485e-5 | 1.94151e-4 |

Table 1 displays relative errors in the estimation of main integral quantities, scaled following (3.36). The relative errors are very small and the mesh containing $N_t = 8599$ triangles is more than enough to ensure a very high precision of the estimates. This mesh density will be used in the following computations. Practically, this criterion is simply achieved for other domains by prescribing the same number of points per unit length in the automatic mesh generator of FreeFem++.

We use in the following the BFGS algorithm to reconstruct Hill's vortex. For sake of simplicity, let $C$ in (3.32) equal to 1 and $a = 1$. In Fig. 3, we show the computational domain. $\Omega_R$ and $\Omega_c$ denote the clipped reconstruction domain and the Hill's vortex domain, respectively. The center of Hill's vortex ring is at (0,0). $\Omega_R$ is defined by a semi-ellipse of half-axis 1.2, centered at (0,0). At the initial stage, $\psi$ is given by the analytic solution (3.33). The regularization strategy proposed in Sec. 3.2.2, coupled with the BFGS algorithm, is used to reconstruct Hill's vortex. The smoothing parameter $\varepsilon$ in (3.27) is chosen equal to $\delta x/2$, with $\delta x$ denoting the mesh scale).

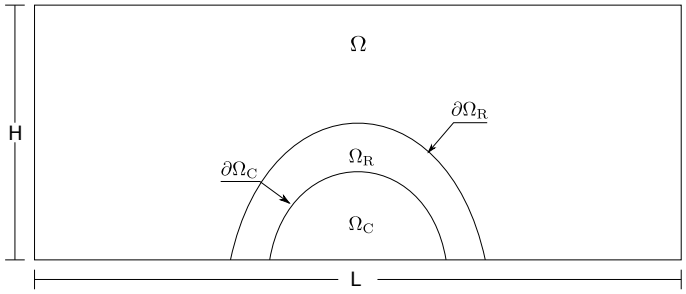


**Figure 3.** Schematic domain for the reconstruction of the Hill's vortex: $L = 6a$ and $H = 3a$.

**Table 2.** Reconstruction of the Hill's vortex. Values of geometrical parameters and integral quantities. "E" and "R" denote "Exact" and "Reconstruction", respectively. $R_{\mathrm{M}} = \sqrt{\mathrm{mean}(|\Omega_c|)/\pi}$.

| | $\delta x$ | $\omega_0$ | $k$ | $R_c$ | $Z_c$ | $R_{\mathrm{M}}$ | $\frac{\Gamma}{Wa}$ | $\frac{I}{Wa^3}$ | $\frac{E}{W^2a^3}$ |
|---|---|---|---|---|---|---|---|---|---|
| E. | \ | 1 | 0 | 0.7071 | 0 | 0.7071 | 5 | $2\pi$ | $3\pi/7$ |
| R. | 0.020 | 1.1778 | 0 | 0.6500 | -0.0109 | 0.6959 | 5.6048 | 6.8153 | 0.9113 |
| | 0.010 | 1.1793 | 0 | 0.7000 | -0.0033 | 0.6983 | 5.6768 | 6.9518 | 0.9731 |
| | 0.005 | 1.0050 | 0 | 0.7064 | -6.23e-5 | 0.6986 | 4.8998 | 6.1365 | 0.7031 |

In Table 2, the reconstructed geometrical parameters and integral quantities are shown with respect to different mesh resolutions. We can notice that the reconstructed values for the geometrical parameters ($R_c$ and $Z_c$) and vortex intensity ($\omega_0$) are improved when fine meshes are used. The deviation of the reconstructed energy $E$ from the exact value is attributed to the smoothing properties of $f_\varepsilon(\psi,k)$ used in the model (3.27). This results in a slightly different representation of the vorticity distribution than the original one. As a consequence, we notice a qualitative deviation of the reconstructed $\psi$ from the exact $\psi$ (see Fig. 4), but a fairly good agreement is obtained for the vortex core geometry and the main integral properties (circulation and impulse). A detailed analysis on the dependence of the quality of results on the smoothing parameter $\varepsilon$ and mesh resolution $\delta x$ will be addressed in a future study.

**3.3.2. Validation using DNS data: reconstruction of the flow field by Gaussian-type vortex models.** We consider in this section the reconstruction of the flow field using Navier-Stokes direct numerical simulation (DNS) data from [9,10] as reference. We use DNS data on the boundary $\partial\Omega_R$ to extract $\psi_{\mathrm{exp}}$ and then apply the BFGS algorithm with vortex ring models (3.25) and (3.26) to recover the stream function inside $\Omega_R$. The reconstructed field is finally compared to original DNS data.

The reconstruction domain $\Omega_R$ is chosen such as the boundary $\partial\Omega_R$ lies in the exterior flow field, *i. e.* $\Omega_b \subset \Omega_R$ in Fig. 1. The convergence tolerance is $10^{-6}$ and the mesh scale $\delta x = 1/25$. The quantities ($\Gamma$, $I$, $E$, $R_c$, $Z_c$) for the reconstructed field are compared to original DNS results in Tab. 3. We can notice that the reconstruction

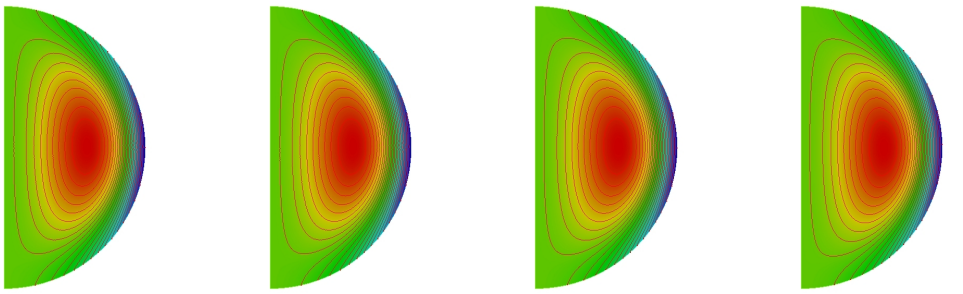

(a) Exact $\psi$ (b) $\delta x = 1/50$ (c) $\delta x = 1/100$ (d) $\delta x = 1/200$

**Figure 4.** Reconstruction of the Hill's vortex. Stream function contours of the analytical solution (a) and reconstructed methods (b-d) for different mesh resolutions $\delta x$ .

**Table 3.** Reconstruction of the Navier-Stokes simulated (DNS) vortex ring. Comparison between the reconstructed results and the DNS results.

| Type | Models | $\Gamma$ | $I$ | E | $R_c$ | $Z_c$ |
|---|---|---|---|---|---|---|
| DNS | Navier-Stokes | 1.17592 | 1.33698 | 0.216944 | 0.66194 | 3.51000 |
| R. | Model (3.25) | 1.17592 | 1.77899 | 0.176575 | 0.66194 | 3.51000 |
| R. | Model (3.26) | 1.17592 | 1.73646 | 0.175927 | 0.65307 | 3.50953 |

algorithm provides a nice approximation to the reference DNS data. In particular, if the elliptical Gaussian distribution in (3.25) is used, the obtained vortex center position is exact for the current problem. For both (3.25) and (3.26), the values of $\Gamma$ are exact and the values of $\omega_0$, $\alpha_R$ and $\alpha_Z$ are slightly different. This was expected, since the models for the vorticity distribution do not exactly match the real vorticity in the DNS vortex ring. In Fig. 5, the stream function contours of the reconstructed $\psi$ are shown against DNS data. We can notice that the results obtained using our models compare very well with the DNS results.

## 4. Conclusion

We have developed a new finite-element BFGS algorithm for the reconstruction of the flow field generated by vortex rings. The algorithm allows to reconstruct the stream function of the flow inside a bounded domain, where the vortex ring is supposed to lie. Using the given information on the boundary of the domain, and supposing a particular model for the vorticity distribution inside the vortex, an optimal control strategy is proposed to compute the parameters of the vortex ring models. The cost function models the match between the reconstructed field and given values of normal derivatives on the boundary. A quasi-Newton Broyden-Fletcher-Goldfarb-Shanno (BFGS) algorithm is derived for this problem and implemented in FreeFem++ using a $P^1$ finite-element spatial discretization. Validation tests using analytical models (Hill's spherical vortex) and Navier-Stokes direct numerical simulation data showed good agreement between reconstructed and reference fields.

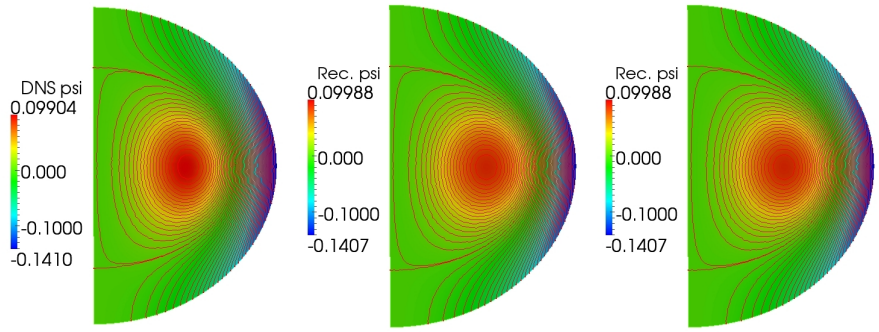


(a) DNS (b) Model (3.25) (c) Model (3.26)

**Figure 5.** Reconstruction of the Navier-Stokes simulated (DNS) vortex ring. Stream function contours of the original DNS field (a) and reconstructed fields using the proposed models for the vorticity distribution (b,c).

Future applications of our algorithm include the flow field reconstruction using experimental data from PIV (Particle Image Velocimetry) of suddenly injected two-phase flows; such flows, generating vortex rings, are obtained during the injection phase in internal combustion (automobile) engines.

## References

[1] D. G. Akhmetov. *Vortex Rings*. Springer-Verlag, Berlin, Heidelberg, 2009.

[2] C. J. Amick and L. E. Fraenkel. The uniqueness of Hill's spherical vortex. *Arch. Rational Mech. Anal.* (1986) **92**, 91–119.

[3] C. J. Amick and L. E. Fraenkel. The uniqueness of a family of vortex rings. *Arch. Rational Mech. Anal.* (1988) **94**, 207–241.

[4] G. K. Batchelor. *An Introduction to Fluid Dynamics*. Cambridge University Press, Cambridge, New York, 7th edition, 1988.

[5] S. Begg, F. Kaplanski, S. Sazhin, M. Hindle, and M. Heikal. Vortex ring-like structures in gasoline fuel sprays under cold-start conditions. *International Journal of Engine Research* (2009)**10**, No. 4, 195–214.

[6] H. Berestycki, E. Fernandez Cara, and R. Glowinski. A numerical study of some questions in vortex ring theory. *RAIRO Analyse numérique*, (1984)**18**, 7–85.

[7] J. Blum, C. Boulbe, and B. Faugeras. Real time reconstruction of plasma equilibrium in a Tokamak. In *International Conference on burning plasma diagnostics, Villa Monastero, Varenna*, 2007.

[8] J. O. Dabiri. Optimal vortex formation as a unifying principle in biological propulsion. *Annual Review of Fluid Mechanics* (2009), **41**, No. 1, 17–33.

[9] I. Danaila and J. Hélie. Numerical simulation of the postformation evolution of a laminar vortex ring. *Phys. Fluids* (2008), **20**, 073602.

[10] I. Danaila, C. Vadean, and S. Danaila. Specified discharge velocity models for the numerical

simulation of laminar vortex rings. *Theor. Comput. Fluid Dynamics* (2009), **23**, 317–332.

[11] I. Danaila and Y. Zhang. Existence and numerical modelling of vortex rings with elliptic boundaries. *submitted*.

[12] A. R. Elcrat, B. Fornberg, and K. G. Miller. Steady axisymmetric vortex flows with swirl and shear. *J. Fluid Mech.* (2008), **613**, 395–410.

[13] M. J. Esteban. Nonlinear elliptic problems in strip–like domains: symmetry of positive vortex rings. *Nonlinear Analysis, Theory, Methods & Applications* (1983), **7**, 365–379.

[14] L. E. Fraenkel. Examples of steady vortex rings of small cross–section in an ideal fluid. *J. Fluid Mech.* (1972), **51**, 119–135.

[15] L. E. Fraenkel and M. S. Berger. A global theory of steady vortex rings in an ideal fluid. *Acta Math.* (1974), **132**, 13–51.

[16] F. Hecht, O. Pironneau, A. Le Hyaric, and K. Ohtsuke. *FreeFem++ (manual)*. www.freefem.org, 2007.

[17] M. J. M. Hill. On a spherical vortex. *Philos. Trans. Roy. Soc. London* (1894), **A185**, 213–245.

[18] S. J. Wright J. Nocedal. *Numerical optimization*. Springer-Verlag, Berlin, New York, 2006.

[19] F. Kaplanski, S. S. Sazhin, S. Begg, Y. Fukumoto, and M. Heikal. Dynamics of vortex rings and spray-induced vortex ring-like structures. *European Journal of Mechanics B/Fluids* (2010), **29**, No. 3, 208–216.

[20] F. B. Kaplanski and Y. A. Rudi. A model for the formation of "optimal" vortex ring taking into account viscosity. *Phys. Fluids* (2005), **17**, 087101.

[21] F. B. Kaplanski, Y. Fukumoto and Y. A. Rudi. Reynolds-number effect on vortex ring evolution in a viscous fluid. *Phys. Fluids* (2012), **24**, 033101.

[22] S. Krueger and M. Gharib. The significance of vortex ring formation on the impulse and thrust of a starting jet. *Phys. Fluids* (2003), **15**, 1271.

[23] H. Lamb. *Hydrodynamics*. Dover, New York, 1932.

[24] K. Mohseni. A formulation for calculating the translational velocity of a vortex ring or pair. *Bioinspiration & Biomimetics* (2006), **1**, S57–S64.

[25] J. Norbury. A steady vortex ring close to Hill's spherical vortex. *Proc. Cambridge Phil. Soc.* (1972), **72**, 253–282.

[26] J. Norbury. A family of steady vortex rings. *J. Fluid Mech.* (1973), **57**, 417–431.

[27] N. A. Pierce and M. B. Giles. An introduction to the adjoint approach to design. *Flow, Turbulence and Combustion* (2000), **65**, No. 3-4, 393–415.

[28] P. G. Saffman. *Vortex Dynamics*. Cambridge University Press, Cambridge, New York, 1992.

[29] D. Thevenin and G. Janiga. *Optimization and computational fluid dynamics*. Springer-Verlag, Berlin, Heidelberg, 2008.